Comparison of Two Navier-Stokes Codes for Attached Transonic Wing Flows

Daryl L. Bonhaus* and Stephen F. Wornom†
NASA Langley Research Center, Hampton, Virginia 23665

In the present study, two codes that solve the three-dimensional thin-layer Navier-Stokes (TLNS) equations are used to compute the steady-state flow for two test cases representing typical finite wings at transonic conditions. The first code, CFL3D, uses an implicit upwind-biased scheme, while the second, TLNS3D, uses an explicit central-difference scheme. Comparisons of computed surface pressure distributions with experimental data and analysis of global aerodynamic coefficient data indicate that for a given grid, CFL3D is more accurate, while TLNS3D is more efficient. To achieve the same level of accuracy, TLNS3D requires more grid points than CFL3D, but converges using slightly less computer time.

Introduction

THIS paper is intended to serve three purposes. First, with the increase in available codes for solving the Reynolds-averaged Navier-Stokes (RANS) equations, and given the high cost of the computer resources required to run these codes routinely, it becomes necessary to evaluate their relative performance to achieve a given accuracy with the least cost in terms of computer resources. Such evaluations have been made of various schemes in two dimensions,[1,2] but comparisons of three-dimensional codes are scarce. Reference 3 is a comparison in three dimensions, but the test case is not a transonic wing flow. Another study[4] compares Euler codes calculating wing-fuselage flows. Conclusions were drawn that are consistent with those stated later in this paper; however, this study focuses more attention on code efficiency.

Second, the study serves as a code-on-code validation and, as will be demonstrated later, it has considerably increased our confidence in both codes. As a byproduct of this comparison, several coding errors were found and corrected in both codes.

Third, the results obtained during the course of this study point to several areas of research that should be considered in the future so that better tools will be available.

Code Descriptions

There are many codes available to compute viscous transonic flow over wings. The Reynolds-averaged Navier-Stokes codes can be divided into two classes of numerical methods. The first class are methods that introduce numerical dissipation through a characteristic decomposition of the inviscid Euler terms and are referred to as upwind or upwind-biased methods. The second class uses central differencing for the flux differences with explicitly added artificial dissipation to eliminate the odd/even decoupling associated with the central-difference method.

Since most of the available codes are primarily research codes, in order to compare the various codes based on these methods, a fair comparison would require these codes to be executing on the same computer and to have the code developers present to provide guidance and make code modifications where required. Since this was not possible for all available codes, the study here was limited to two codes developed at NASA Langley where the code developers were present to monitor the results obtained with their codes.

The codes analyzed are referred to as CFL3D and TLNS3D and both represent the state of the art for the upwind and central-difference methodologies, respectively. Both use a finite volume formulation, with flow quantities stored at cell centers, to integrate the three-dimensional time-dependent TLNS equations in time until a steady-state solution is reached. To accelerate convergence, both codes can make use of grid sequencing, multigrid, and local time-stepping techniques.

CFL3D uses the Pulliam-Chaussee diagonal ADI time-marching algorithm[5] with third-order upwind-biased differences for the spatial derivatives of the inviscid terms. The upwind method used is the Roe flux-difference-splitting (FDS) scheme.[6] A min-mod flux limiting scheme is employed to obtain smooth solutions in the vicinity of discontinuities. During the investigations conducted here, it was determined that the multigrid feature did not improve convergence for Navier-Stokes solutions and it was not used. Details on the formulation of this code can be found in Refs. 3 and 7–10.

TLNS3D uses an explicit five-stage Runge-Kutta time-marching algorithm, with second-order central differences for the spatial derivatives. A blend of second- and fourth-order artificial dissipation terms are added to maintain numerical stability. The artificial dissipation terms are scaler. In addition to the previously mentioned convergence acceleration techniques, TLNS3D utilizes implicit residual smoothing to improve convergence to steady state. Details on the formulation of this code can be found in Refs. 3 and 11–19.

For turbulent attached flows, both codes uses the Baldwin-Lomax algebraic turbulence model.[20] TLNS3D also has the option to use the Johnson-King nonequilibrium turbulence model[21] that has been shown to produce more accurate solutions for separated flows.[17]

With the exception of the downstream boundary, the boundary conditions in both codes are mathematically the same. The wing surface is modeled as a viscous surface with a no-slip condition on velocity and a zero normal pressure gradient. The treatment of the far-field boundaries is based on Riemann invariants for one-dimensional flow normal to

Received May 29, 1990; revision received March 12, 1991; accepted for publication March 12, 1991.

*Research Scientist, Computational Aerodynamics Branch, Fluid Mechanics Division. Member AIAA.

†Research Scientist, Theoretical Flow Physics Branch, Fluid Mechanics Division; currently at Principia Recherche Developpement, B.P. 122 Sophia Antipolis, 06561 Valbonne Cedex (France). Member AIAA.

the boundary as described in Ref. 22. These conditions are also used for the downstream boundary in CFL3D. In TLNS3D, the flow quantities at the downstream boundary are determined by extrapolation. Symmetry conditions are imposed on the grid plane at the wing root plane. The only other difference between the codes was the location of the transition point, which for TLNS3D was set at 2% chord on both the upper and lower surfaces. For CFL3D, the flow was assumed to be turbulent over the entire wing.

Test Case Descriptions

The test cases used for analysis are the ONERA M6 Wing[23] and the Lockheed Wing B[24] configuration. The geometrical characteristics of both wings can be found in Ref. 25. The M6 wing was developed specifically for experimental support of three-dimensional transonic and subsonic flowfield studies, and an extensive data base of surface pressure distributions is available over a range of transonic Mach numbers at angles of attack up to 6 deg. The particular case analyzed in this study is for a Mach number of 0.84 and an angle of attack of 3.06 deg.

The Lockheed Wing B configuration was also tested for the purpose of computational fluid dynamic (CFD) code evaluation. In addition to a data base of surface pressure distributions similar to that available for the ONERA M6, experimental force and moment coefficients and spanwise lift distributions are also available for Wing B. The case examined in this study is for a Mach number of 0.851 and an angle of attack of 2.95 deg.

Because CFL3D does not have the option of using the Johnson-King turbulence model that has been shown to be more accurate for separated flows, only attached flow cases were selected and both codes used the Baldwin-Lomax turbulence model.

Four computational grids were generated for each wing using a two-boundary transfinite interpolation technique.[26] These grids are of C-O topology (C in the streamwise direction and O in the spanwise direction). The finest grid contains 289 points in the streamwise direction, 65 points in the direction normal to the wing surface, and 49 points in the crossflow direction (i.e., 289 × 65 × 49). The other grids are (in decreasing order by size) 193 × 49 × 33, 145 × 33 × 25, and 97 × 25 × 17. On the lower surface of the wing, the trailing edge was located at i = 33, 25, 17, and 13, respectively, where i = 1 corresponds to the far downstream lower surface location. On the upper surface, the trailing edge was located at 257, 169, 129, and 85. This translates into the following number of cells on each surface: 21,728, 9216, 5376, and 2304.

The outer boundary of the computational domain extends approximately 6.25 semispans vertically (above and below the wing), 6.5 semispans upstream, 7.5 semispans downstream, and 6.5 semispans horizontally outward from the wing tip. The physical geometric coordinates are scaled so that the semispan of the wing in the computational domain is of unit length.

Results

First, the effect of grid refinement on the section pressure coefficients is examined. Next, the iteration history and the accuracy for a given grid is presented. Then, after an examination of the spanwise lift distributions, a discussion of relative efficiency to achieve a given accuracy and the conclusions follow.

Surface Pressure

Figure 1 shows the effect of grid refinement on the pressure distributions for CFL3D and TLNS3D, respectively, for the ONERA M6 Wing. The spanwise distance Y is normalized with respect to the semispan length $B/2$. Figure 2 shows the corresponding results for the Lockheed Wing B. Figures 1 and 2 show distinctively different convergence patterns be-

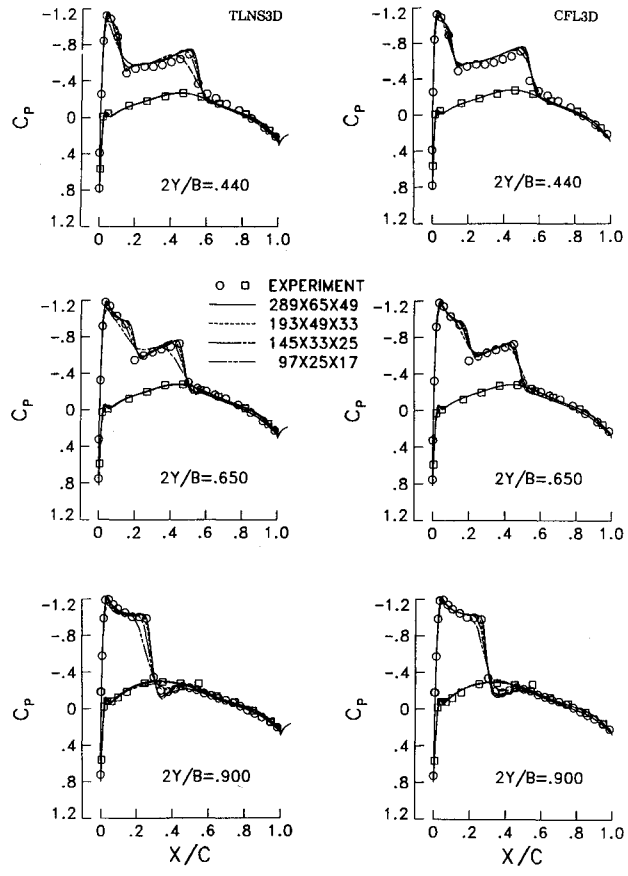

Fig. 1 Effect of grid refinement on pressure coefficient for the M6 wing.

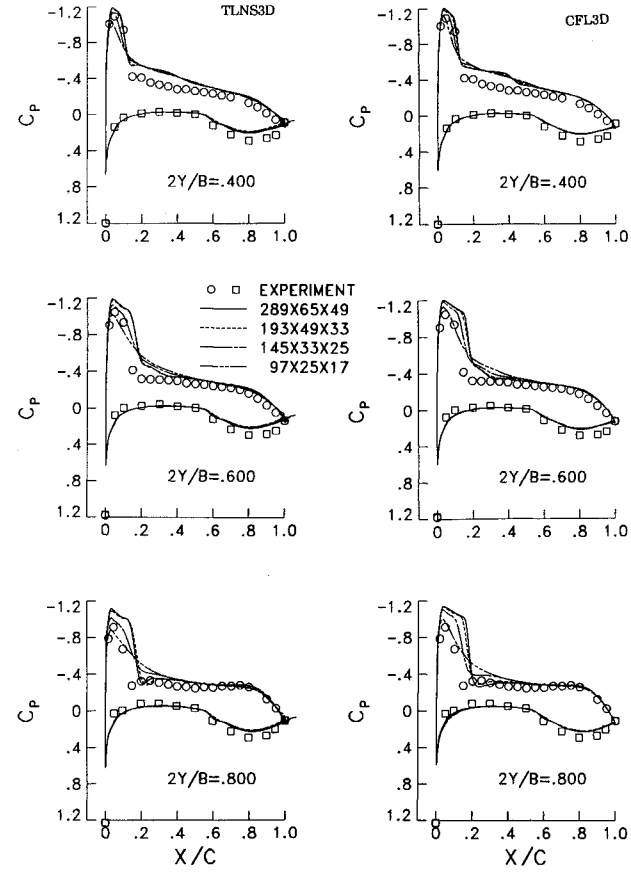

Fig. 2 Effect of grid refinement on pressure coefficient for Wing B.

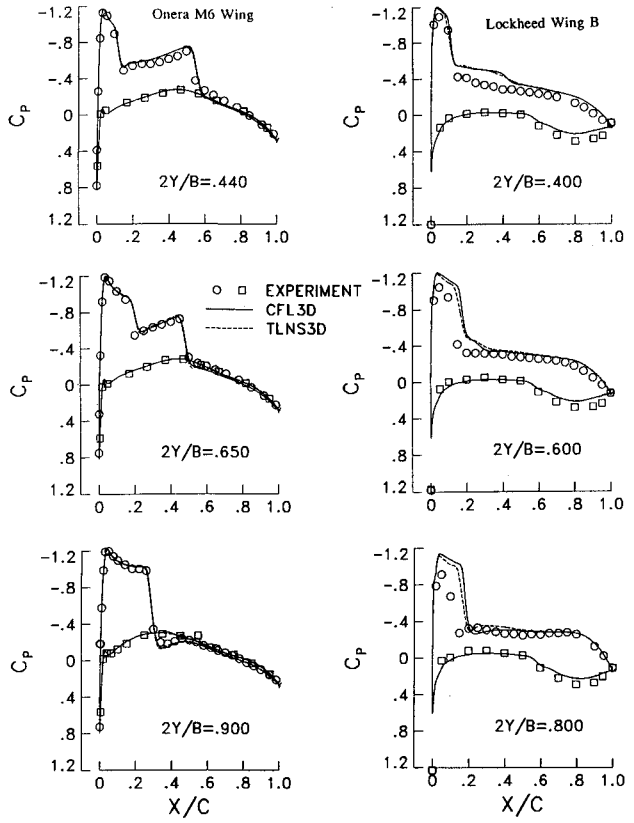

Fig. 3 Comparisons of pressure coefficient on the 289 × 65 × 49 grid.

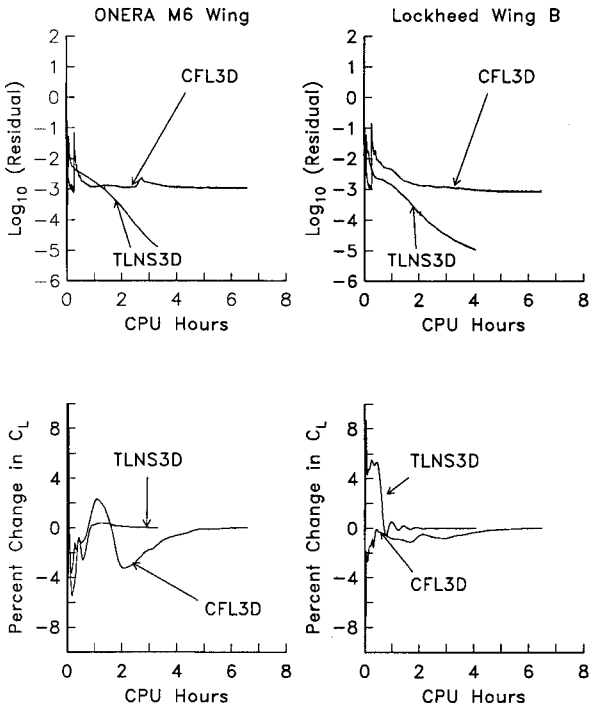

Fig. 4 Convergence histories for 289 × 65 × 49 grid.

tween TLNS3D and CFL3D as the grid is refined. For the ONERA M6 Wing, CFL3D predicts approximately the same shock thickness on each grid. The changes that do occur with grid refinement are reflected more in improved resolution of the region of accelerated flow near the leading edge than in shock resolution. For TLNS3D, the effect of grid refinement is to sharpen the shock as well as to resolve the region of accelerated flow at the leading edge. For the Lockheed Wing

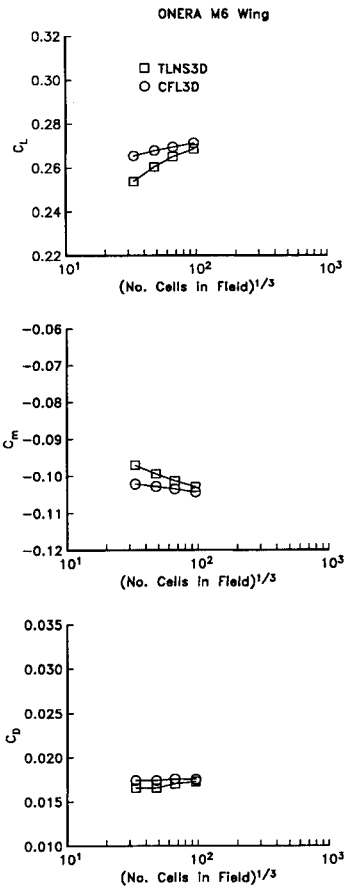

Fig. 5a Values of force and moment coefficients for the M6 wing.

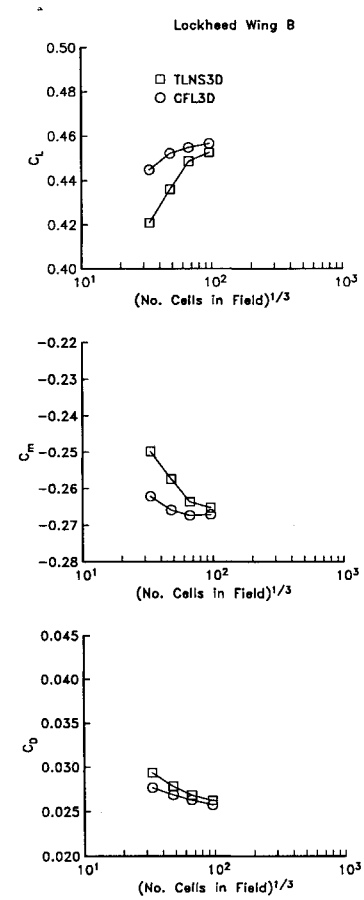

Fig. 5b Values of force and moment coefficients for Wing B.

B, both CFL3D and TLNS3D predict shocks that sharpen as the grid is refined.

Figure 3 shows comparisons of the computed pressure distributions on each individual wing for the 289 × 65 × 49 grid. There is good agreement between the calculations for the ONERA M6 on the finest mesh. For the Lockheed Wing B, there are substantial differences between grid-refined calculations and the experimental data. This is due to wind-tunnel wall effects in the experiment which have not been considered in the calculations. Reference 24 gives estimated Mach-number and angle-of-attack corrections but they have not been used here. Angle-of-attack corrections are on the order of one degree. In addition, after the calculations were performed, an error in the computational geometry was found. The wing on which the calculations were performed was swept approximately 5 deg farther aft than the wind-tunnel geometry. Because of the magnitude of the angle-of-attack corrections, however, it is not expected that correcting the geometry would result in better agreement with the experiment. The conclusions drawn about the relative performance of the two codes are still valid.

Iteration History

In order to examine the relative efficiency and accuracy of the codes, the values of the force coefficients are stored at each iteration. Using these data, the percent changes in the force coefficients at each iteration are calculated using their final converged values as references. CPU time, or the time required to run the code if it were the only task being performed by the computer, is stored at the end of each grid sequence. This time includes the time required to read and write data files and the time required to perform the calculations. It does not include code compilation time or post-processing time. In this manner, the amount of CPU time required for the force coefficients to converge to a given percentage of their final values is determined.

The convergence histories for the continuity equation residual and the lift coefficient using the 289 × 65 × 49 grid are presented in Fig. 4. For each grid, the residual for CFL3D drops approximately three orders of magnitude before leveling off and exhibiting high-frequency oscillations that are attributed to the use of the flux limiter. For TLNS3D, the residual continues to decrease to the end of the run.

Figure 4 clearly illustrates the strong point of TLNS3D, that is, faster convergence of the residual and the integrated force coefficients as the grid is refined. The convergence histories for the 97 × 25 × 17 and the 145 × 33 × 25 grids showed the same approximate rate of convergence for both codes. As the number of grid points becomes large, the 193 × 49 × 33 and 289 × 65 × 49 grids, TLNS3D is more efficient than CFL3D. This is an important advantage since run times for fine grids are measured in hours as opposed to minutes on the coarser meshes.

To quantify the relative efficiency for a given grid, it is assumed that convergence is acceptable when the percent changes in the lift, viscous drag, and pressure drag convergence histories are less than 1/2%. To reach this criterion, CFL3D requires on the order of twice the CPU time of TLNS3D for the two finest grids. For the 193 × 49 × 33 grid, this translates into approximately 40–50 min additional CPU time. For the 289 × 65 × 49 grid, this translates into 2–3 h additional CPU time.

Accuracy

The values of the coefficients of lift, pitching moment, and total drag for each wing are shown in Fig. 5. The values given for CFL3D on the two finest grids are accurate to three decimal places. To estimate errors, reference values for the force coefficients must be known. These can be the experimental values or the values from a numerical solution using a very fine grid. For these test cases, the experimental values are not known. Limits on computer resources did not permit so-

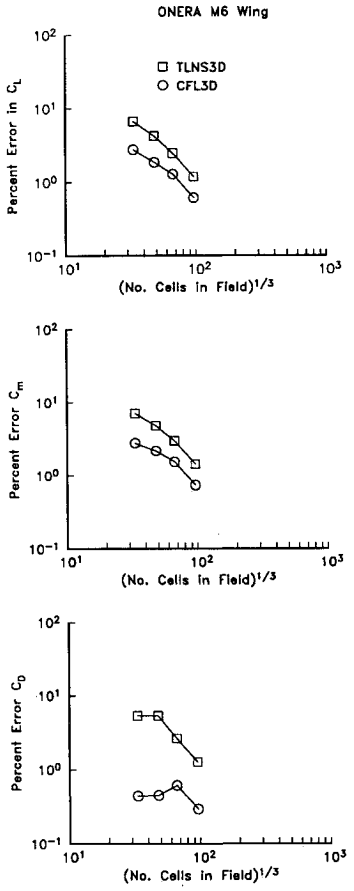

Fig. 6a Numerical error in force and moment coefficients for the M6 wing.

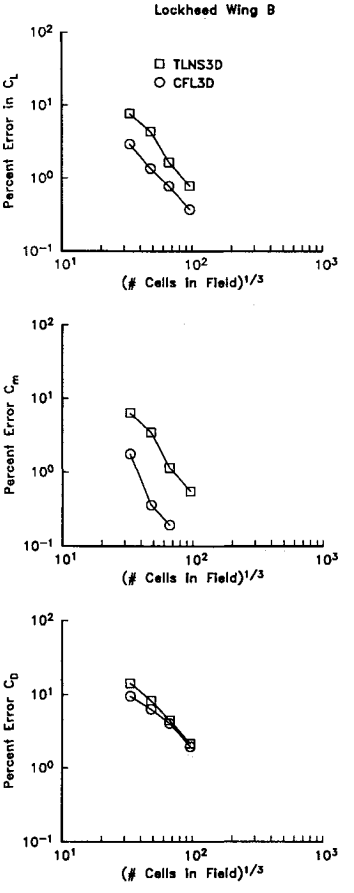

Fig. 6b Numerical error in force and moment coefficients for Wing B.

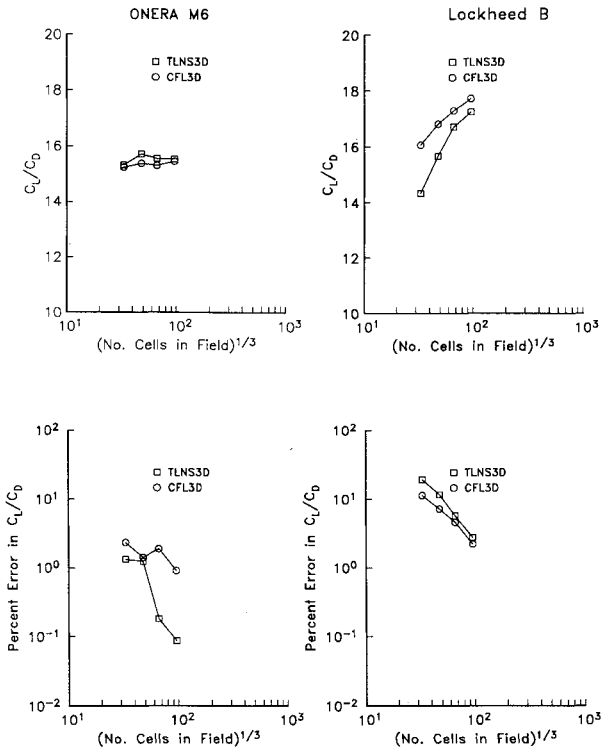

Fig. 7 Values of and numerical error in lift-to-drag ratio.

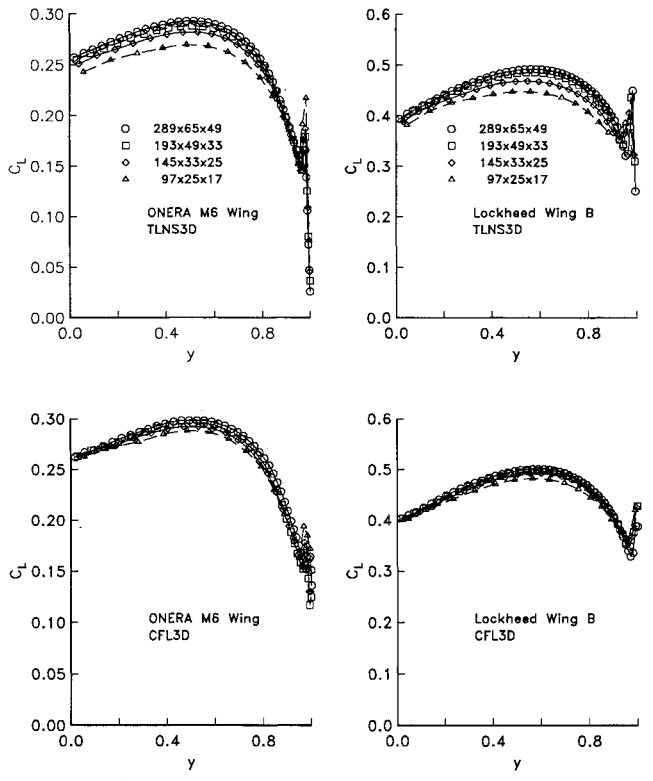

Fig. 8 Effect of grid refinement on spanwise lift distribution.

lutions on more refined meshes; therefore, a second-order Richardson extrapolation was used based on the cube root of the total number of cells in the field. The finest two levels of mesh refinement were used in this extrapolation. The numerical error was then calculated using these extrapolated values as reference.

Figure 6 shows the percentage error in the lift, pitching moment, and the total drag. The error distributions for the lift and pitching moment shown in Fig. 6 are classic examples of what one would expect to see from second-order schemes,

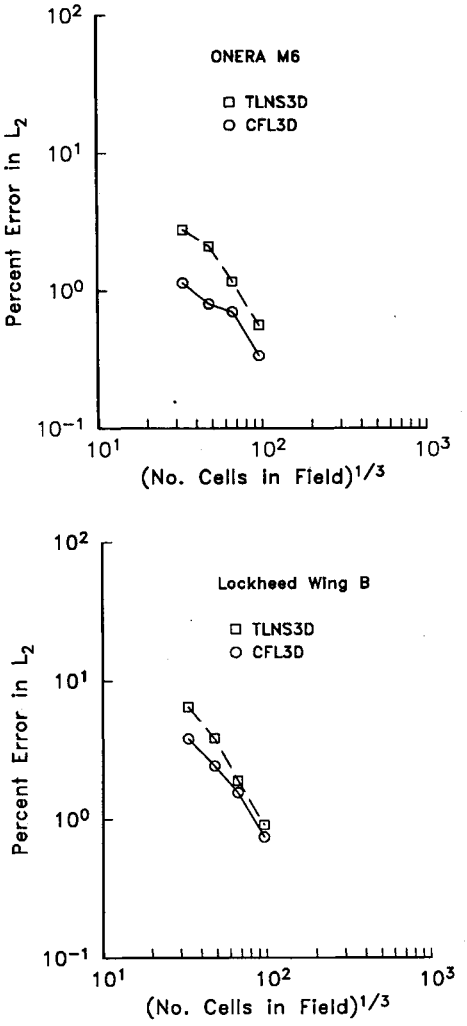

Fig. 9 L_2 spatial error norm.

that is, as the grid is refined, the error decreases in a consistent manner asymptotic to a line of slope 2. These figures show CFL3D to be the more accurate scheme for predicting the lift and pitching moment.

The errors in the total drag for the ONERA M6 show CFL3D to be significantly more accurate than TLNS3D and relatively insensitive to grid refinement. Because this same behavior is not observed for the Lockheed Wing B, where CFL3D is slightly more accurate, it is believed that this is related to the accurate predicted shock thickness on each grid obtained with CFL3D for the ONERA M6 case. For the Lockheed Wing B, both codes predict shocks that sharpen as the mesh is refined leading to total drag error predictions of the same order.

Shown in Fig. 6 are the values of the lift, pitching moment, and total drag for each wing. The percent differences in the predicted infinite-grid values of lift, pitching moment, total drag, and lift-to-drag ratio between the two codes were -0.4, -0.6, 0.1, and -0.5 for the ONERA M6 Wing and -0.5, -0.0, -1.6, and -2.1 for the Lockheed Wing B. The percent differences are with reference to CLF3D.

Figure 7 shows the lift-to-drag ratios and their errors with grid refinement. As can be seen, TLNS3D is significantly more accurate than CFL3D in predicting the lift-to-drag ratio for the ONERA M6 Wing and is slightly less accurate for the Lockheed Wing B. That is, although CFL3D predicts more accurate individual values of the lift and total drag on a given grid for the ONERA M6 Wing, TLNS3D predicts the more accurate value of the lift-to- drag ratio.

A similar anomaly occurs for the total drag where it is noted that, in general, the error in the total drag for both codes is

smaller than the error in each of the individual components that are added to obtain the total drag.

Spanwise Lift Distributions

Figure 8 shows the convergence of the lift distributions with grid refinement. CFL3D shows less variation than TLNS3D with grid refinement. One noticeable difference between the two codes is the symmetry plane values of the lift. CFL3D shows very little variation at the symmetry plane in comparison with TLNS3D. Also, CFL3D shows a change in the slope of the lift distribution as the symmetry plane is approached.

Relative Efficiency for a Given Accuracy

One of the goals of this work was to examine the relative efficiency of TLNS3D and CFL3D to achieve a given accuracy. This is not a simple task due to distinctly different trends observed for the two test cases and the lack of exact values of the force coefficients on which to base the error estimates.

In order to determine the relative efficiency for a given accuracy, various viewpoints are considered. The wing designer is primarily interested in obtaining accurate values for the lift-to-drag ratio whereas the propulsion designer is interested in the total drag. Both of the viewpoints are different from that of the structural engineer who is interested in the lift and pitching moment coefficients. In order to have a single measure of accuracy that reflects the different viewpoints, accuracy is examined in terms of the L_2 norm computed using the percent error in lift, pitching moment, total drag, and the lift-to-drag ratio. This norm is shown in Fig. 9. Using this norm, CFL3D is the more accurate code on a given grid. To quantify this, the accuracy achieved with TLNS3D using the 289 × 65 × 49 grid (884,736 cells) for the ONERA M6 Wing could have been obtained with CFL3D using 511,113 cells or 42% fewer cells A calculation for this grid was not available. However, a solution is available on a grid that has 67% fewer cells (the 193 × 49 × 33 grid) and can be used to estimate the relative efficiency on a grid with 42% fewer calls.

Shown in Fig. 10 are the convergence histories for CFL3D using the 193 × 49 × 33 grid (67% fewer cells) and TLNS3D using the 289 × 65 × 49 grid. It is concluded that TLNS3D is as efficient as CFL3D even though the CFL3D calculation was made with a grid containing 67% fewer cells. It follows, then, that TLNS3D is significantly more efficient than CFL3D if CFL3D is run on a grid having 42% fewer cells than the grid used for TLNS3D; therefore, TLNS3D is more efficient than CFL3D in attaining the same accuracy.

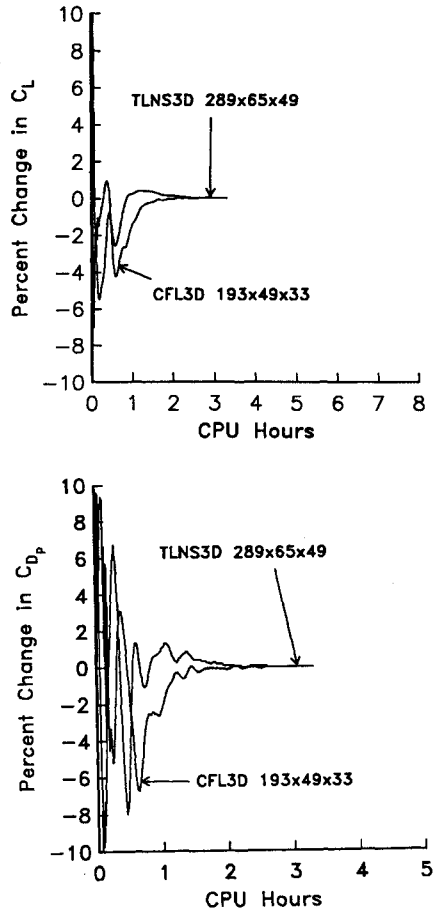

Fig. 10 Relative efficiency for the M6 wing.

Conclusions

Based on the numerical results for the ONERA M6 Wing and the Lockheed Wing B, for attached transonic flow, the following are concluded:

1) In general, CFL3D is the more accurate code for a given grid.

2) For a given grid, TLNS3D is the more efficient code, especially as the number of grid points becomes large. For the finest grid considered here (884,736 cells), it is approximately twice as efficient.

3) For equivalent accuracy, TLNS3D is the more efficient code.

All error estimates were based on the infinite grid values obtained using Richardson extrapolation. For the ONERA M6, the pressure coefficients showed excellent agreement on the finest grid and the differences between the infinite grid values were small. For the Lockheed Wing B, there were significant differences in the pressure coefficients that in turn are reflected in significant differences in the infinite grid values. For these reasons, further comparisons with other codes and more detailed experimental data are suggested.

The results presented here also suggest potential improvements in both methods. First, a smoother flux-limiting function for CFL3D would improve convergence of the residual, and the development and application of a multigrid capability would also accelerate convergence. CFL3D is capable of running multigrid, but the current implementation improves convergence only for inviscid calculations. The obvious need with regard to TLNS3D is improved grid convergence. This may be accomplished with improved dissipation models to mimic the grid convergence of upwind methods.

Acknowledgments

The authors would like to acknowledge the contributions of James L. Thomas and Veer N. Vatsa for questions relating to CFL3D and TLNS3D. The authors would also like to thank Manuel D. Salas who suggested the idea of comparing the two codes and for fruitful discussion of the results.

References

[1]Swanson, R. C., and Turkel, E., "On Central-Difference and Upwind Schemes," NASA CR-182061, June 1990.

[2]Maksymiuk, C. M., Swanson, R. C., and Pulliam, T. H., "A Comparison of Two Central-Difference Schemes for Solving the Navier-Stokes Equations," NASA TM-102815, July 1990.

[3]Vatsa, V. N., Thomas, J. L., and Wedan, B. W., "Navier- Stokes Computation of a Prolate Spheroid at Angle of Attack," AIAA Paper 87-2627-CP, Aug. 1987; see also *Journal of Aircraft*, Vol. 26, Nov. 1989, pp. 986–993.

[4]Agrawal, S., Lowrie, R. B., and Creasman, S. F., "An Evaluation of Euler Solvers for Transonic Computations on Wing-Fuselage Geometries," AIAA 8th Applied Aerodynamics Conference, AIAA Paper 90-3015, Portland, OR, Aug. 1990.

[5]Pulliam, T. H., and Chaussee, D. S., "A Diagonal Form of an Implicit Approximate Factorization Algorithm," *Journal of Computational Physics*, Vol. 39, No. 2, 1981, pp. 347–363.

[6]Roe, P. L., "Characteristic-Based Schemes for the Euler Equations," *Annual Review of Fluid Mechanics*, 1986, pp. 337–365.

[7]Thomas, J. L., Van Leer, B., and Walters, R. W., "Implicit Flux-Split Schemes for the Euler Equations," AIAA Paper 85-1680, July 1985; see also *AIAA Journal*, Vol. 28, June 1990, pp. 973–974.

[8]Thomas, J. L,, Taylor, S. L., and Anderson, W. K., "Navier-

Stokes Computations of Vortical Flows Over Low-Aspect-Ratio Wings," AIAA Paper 87-0207, 1987; see also *AIAA Journal*, Vol. 28, Feb. 1990, pp. 205–212.

[9]Van Leer, B., Thomas, J. L., Roe, P. L., and Newsome, R. W., "A Comparison of Numerical Flux Formulas for the Euler and Navier-Stokes Equations," AIAA 8th Computational Fluid Dynamics Conference, AIAA Paper 87-1104-CP, June 1987.

[10]Van Leer, B., "Upwind-Difference Methods for Aerodynamic Problems Governed by the Euler Equations," *Lectures in Applied Mathematics*, Vol. 22, 1985, pp. 327–336.

[11]Jameson, A., Schmidt, W., and Turkel, E., "Numerical Solutions of the Euler Equations by Finite-Volume Methods Using Runge-Kutta Time-Stepping Techniques," AIAA 14th Fluid and Plasma Dynamics Conference, AIAA Paper 81-1259, Palo Alto, CA, 1981.

[12]Jameson, A., and Baker, T. J., "Improvements to the Aircraft Euler Method," AIAA 25th Aerospace Sciences Meeting, AIAA Paper 87-0452, Reno, NV, Jan. 1987.

[13]Swanson, R. C., Turkel, E., "A Multistage Time- Stepping Scheme for the Navier-Stokes Equations," AIAA 23rd Aerospace Sciences Meeting, AIAA Paper 85-0035, Reno, NV, Jan. 1985.

[14]Vatsa, V. N., "Accurate Numerical Solutions for Transonic Viscous Flows Over Finite Wings," *Journal of Aircraft*, Vol. 24, June 1987, pp. 377–385.

[15]Vatsa, V. N., and Wedan, B. W., "Navier-Stokes Solutions for Transonic Flow Over a Wing Mounted in a Tunnel," AIAA Paper 88-0102, Jan. 1988; see also *Journal of Aircraft*, Vol. 26, Feb. 1989, pp. 157–161.

[16]Martinelli, L., "Calculation of Viscous Flows with Multigrid Methods," Ph.D. Dissertation, MAE Dept., Princeton Univ., Princeton, N.J.

[17]Abid, R., Vatsa, V. N., Johnson, D. A., and Wedan, B. W., "Prediction of Separated Transonic Wing Flows with a Nonequilibrium Algebraic Model," AIAA Paper 89-0558, Jan. 1989; see also *AIAA Journal*, Vol. 28, Aug. 1990, pp. 1426–1431.

[18]Vatsa, V. N., and Wedan, B. W., "Development of an Efficient Multigrid Code for 3-D Navier-Stokes Equations," AIAA Paper 89-1791, June 1989; see also *Computers & Fluids*, Vol. 18, No. 4, 1990, pp. 391–403.

[19]Turkel, E., and Vatsa, V. N., "Effect of Artificial Viscosity on Three-Dimensional Flow Solutions," AIAA 21st Fluid Dynamics, Plasma Dynamics and Lasers Conference, AIAA Paper 90-1444, Seattle, WA, June 1990.

[20]Baldwin, B. S., and Lomax, H., "Thin-Layer Approximation and Algebraic Model for Separated Turbulent Flows," AIAA 16th Aerospace Sciences Meeting, AL, AIAA Paper 78-257, Huntsville, AL, 1978.

[21]Johnson, D. A., and King, L. S., "A Mathematically Simple Turbulence Closure Model for Attached and Separated Turbulent Boundary Layers," *AIAA Journal*, Vol. 23, No. 11, 1985, pp. 1684–1692.

[22]Thomas, J. L., and Salas, M. D., "Far-Field Boundary Conditions for Transonic Lifting Solutions to the Euler Equations," *AIAA Journal*, Vol. 24, No. 7, 1986, pp. 1074–1080.

[23]Schmitt, V., and Charpin, F., "Pressure Distributions on the ONERA M6 Wing at Transonic Mach Numbers," AGARD-AR-138, Chap. B-1, May 1979.

[24]Hinson, B. L., and Burdges, K. P., "Acquisition and Application of Transonic Wing and Far-Field Test Data for Three- Dimensional Computational Method Evaluation," Air Force Office of Scientific Research, AFOSR-TR-80-0421, Vols. 1 & 2, March 1980.

[25]Bonhaus, D. L., and Wornom, S. F., "Relative Efficiency and Accuracy of Two Navier-Stokes Codes for Attached Transonic Wing Calculations," NASA TP-3061, Feb. 1991.

[26]Eriksson, L.-E., "Transfinite Mesh Generation and Computer-Aided Analysis of Mesh Effects," Ph.D. Dissertation, Uppsala Univ., Sweden, 1984.